Journal of King Saud University – Engineering Sciences (2025) 37:5
https://doi.org/10.1007/s44444-025-00007-9

ORIGINAL PAPER

Facile synthesis of reduced graphene oxide using natural plant extracts as green reducing agents

A. Muhammad Afdhal Saputra[1,2] · Marpongahtun[2,3] · Andriayani[2,3] · Ronn Goei[4] · Alfred Iing Yoong Tok[4] · Stergios Goutianos[5] · Saharman Gea[2,3]

Received: 21 January 2025 / Accepted: 28 April 2025 / Published online: 5 June 2025
© The Author(s) 2025

Abstract

Reduced graphene oxide (rGO) was successfully synthesized using environmentally friendly reducing agents derived from natural sources including *Zanthoxylum acanthopodium* (andaliman), *Murraya paniculata* (kemuning leaves), *Psidium guajava* (guava leaves), and *Miconia crenata* (senduduk bulu)—via a modified Hummers method. The structural and physicochemical properties of the synthesized materials were characterized using X-ray diffraction (XRD), Fourier transform infrared spectroscopy (FTIR), ultraviolet–visible (UV–Vis) spectroscopy, scanning electron microscopy (SEM), Brunauer–Emmett–Teller (BET) analysis, and electrochemical techniques. XRD analysis revealed a shift in the characteristic GO peak from 11.04° to higher angles (21.79°–26.00°), confirming successful reduction. FTIR spectroscopy demonstrated reduction efficiency of 42.28%–52.63%, while UV–Vis spectra exhibited a redshift in absorption peaks, indicating restored π-electron conjugation. SEM images showed aggregated, wrinkled morphology with exfoliated sheets, and BET analysis confirmed mesoporosity (pore diameters 2–50 nm). Electrochemical studies revealed excellent linear correlations ($R^2 > 0.99$), highlighting efficient electron transfer. This work underscores the potential of plant-derived reductants as sustainable alternatives for high-quality rGO synthesis, suitable for advanced electrochemical applications.

Keywords Reduced graphene oxide · Green synthesis · Natural reducing agents · Electrochemical properties · Sustainable materials

1 Introduction

Graphene and its derivatives, such as graphene oxide (GO) and reduced graphene oxide (rGO), are composed of a single two-dimensional layer of carbon atoms (Chandra Mohan Kurmarayuni, Krishna Kumari, Srikanth, and Kurapati 2024). These materials exhibit exceptional electronic, thermal (Farooq, et al. 2024), mechanical (Jovanovic, et al. 2024), and optical properties (T. N 2024). Although various methods—such as liquid-phase exfoliation, mechanical exfoliation (Yip and Tong 2023), epitaxial growth on silicon carbide (Othman et al. 2022), chemical vapor deposition (CVD) (Zhang, et al. 2022), and chemical oxidation–reduction—have been employed to synthesize single-layer graphene (Singh et al. Apr. 2023; Khan and Shaida 2023), only the chemical oxidation–reduction route has been commercialized, owing to its capacity for large-scale production of high-quality graphene (Khan and Shaida 2023). Graphene and its derivatives possess a remarkably high surface area of approximately 2630 m^2/g (Zhang et al. 2020), making them

✉ Saharman Gea
s.gea@usu.ac.id

1 Postgraduate School, Department of Chemistry, Faculty of Mathematics and Natural Sciences, Universitas Sumatera Utara, Jl. Bioteknologi No. 1, Medan 20155, Indonesia

2 Cellulosic and Functional Material Research Center, Universitas Sumatera Utara, Jl. Bioteknologi No.1, Medan 20155, Indonesia

3 Department of Chemistry, Faculty of Mathematics and Natural Sciences, Universitas Sumatera Utara, Jl. Bioteknologi No.1, Medan 20115, Indonesia

4 School of Materials Science and Engineering, Nanyang Technological University, 50 Nanyang Avenue, Singapore 639798, Singapore

5 Department of Manufacturing and Civil Engineering, Norwegian University of Science and Technology, NO-2802 Gjøvik, Norway

highly desirable for a broad range of applications, including electronics, catalysis (Kumari and Bhandari 2024), chemical sensing (Mahalingam et al. 2023), drug delivery (Kumar et al. 2023), and as active components in nanocomposites. Graphite consists of multiple layers of covalently bonded carbon atoms, from which graphene is derived as a single, isolated layer (Patra et al. 2017). GO is rich in oxygen-containing hydrophilic functional groups such as hydroxyl, carboxyl, epoxy, and carbonyl, making it highly dispersible in aqueous media (Makaudi et al. 2023). In contrast, rGO is produced through a reduction process that significantly decreases the presence of these functional groups, thereby restoring partial conductivity and enhancing its electrochemical properties (Liu et al. 2022). Although the production of pristine graphene with nearly 100% single-layer content remains challenging and expensive, rGO is often favored for practical applications due to its relatively simple synthesis and tunable properties (Asih 2019; Baqiya et al. 2020).

The chemical oxidation of graphite into graphene oxide can be performed through several methods, including the Brodie (Brodie 1960), Staudenmaier (Staudenmaier 1898), Hummers (Hummers and Offeman 1958), and modified Hummers methods (Alam et al. 2017). Among these, the Hummers method is particularly preferred due to its ability to complete the reaction in a few hours, replacing the hazardous $KClO_3$ with $KMnO_4$ to introduce oxygenated functional groups into the graphite structure. The interlayer van der Waals forces are weakened by the introduction of oxygenated functional groups into the graphite structure (Chong et al. 2015). In addition, the use of $KMnO_4$ enhances the safety of the GO synthesis process (Liu et al. 2018), while the replacement of fuming HNO_3 with $NaNO_3$ effectively eliminates the formation of hazardous acid mist (Alam et al. 2017). Despite its advantages, however, the Hummers method still has some drawbacks, such as the release of toxic gases like NO_2 and N_2O_4 and the difficulty in removing residual Na^+ and NO_3^- ions from the wastewater generated during the synthesis and purification of GO. In this study, we modified the traditional Hummers method to increase product yield and reduce toxic gas emissions by adjusting the proportions of $KMnO_4$ and H_2SO_4 used, making the process more efficient and environmentally friendly.

The process of reducing GO to rGO involves breaking C–OH bonds, which makes it easier to reconstruct C–C bonds (Liu and Speranza 2022). The use of chemicals such as hydrazine hydrate, sodium borohydride, and hydroquinone, which are classified as powerful reductants, is common in this reduction process (Shayeghi Sabzevar and M. M. Bagheri – Mohagheghi, and A. Shirpay 2022; Anju and Renuka 2019; Panicker and Sahu 2021). However, recent studies have explored new approaches for developing environmentally friendly reducing agents, such as *Thuja orientalis* (Kumar et al. 2021), oil palm leaf extract (Amir Faiz et al. 2020), nettle leaf extract (Mahmudzadeh et al. 2019), eucalyptus leaf extract (Jin et al. 2018), soursop leaf extract (*Annona muricata*) (Fatimah et al. 2022), pomelo (*Citrus maxima*), and *Tamarindus indica* extract (Panicker and Sahu 2021), to address the hazardous nature of hydrazine. These green reductants are natural antioxidants that are nontoxic and possess high reducing potential, making them ideal alternatives to hydrazine (Faniyi, et al. 2019). While ascorbic acid has been widely used for the production of rGO, limited research has been conducted on the use of other green reducing agents, such as plant extracts, in this process. The presence of active compounds such as aporphine, isoquinoline, chlorogenic acid, enzymes, chelating agents, vitamins, and mono-epoxy functional groups in the leaf extract has the potential to reduce and chemically modify the surface of GO (Jin et al. 2018). For instance, hydroxyl functional groups from phenolic structures can facilitate the removal of oxygenated functionalities through a reduction mechanism (Fatimah et al. 2022; Ramanathan et al. 2021).

Fatimah et al. (2022) synthesized rGO sheets using Annona muricata extract as a reducing agent. They employed a modified Hummers method incorporating $NaNO_3$ to synthesize GO. Their results demonstrated a reduction efficiency of 86.85% with a reduction time of 24 h (Fatimah et al. 2022). Similarly, Bhattacharya et al. (2017) achieved reduction efficiency of 72.51% using *Aloe vera* as the reducing agent (Bhattacharya et al. 2017). In another study, Chen et al. (2018) produced GO using a modified Hummers process and subsequently reduced it to rGO using ascorbic acid. Their findings indicated successful elimination of oxygen groups, confirming the efficacy of the reduction process (Chen et al. 2018).

This study adopts an environmentally friendly approach for the synthesis of GO and its subsequent reduction. The oxidation process was conducted using a modified Hummers method, a greener alternative that replaces fuming HNO_3 with $NaNO_3$, thereby eliminating acid mist formation and enhancing safety. GO was subsequently reduced to produce rGO using natural reducing agents derived from plant extracts of *Zanthoxylum acanthopodium* (andaliman), *Murraya paniculata* (kemuning leaves), *Psidium guajava* (guava leaves), and *Miconia crenata* (senduduk bulu). The methodology employed is relatively straightforward and potentially scalable for large-scale rGO production. However, a significant challenge remains in producing monolayer graphene, as the process typically yields few-layer or multilayer rGO with residual oxygen-containing functional groups.

Unlike previous studies that often focused on a single type of plant extract or commercial reductants such as ascorbic acid, this research provides a comprehensive comparative evaluation across multiple tropical plant species within a unified experimental framework. This approach not only leverages underutilized local biodiversity but also offers novel

insights into the relationship between reduction efficiency, structural transformation, and electrochemical performance of the resulting rGO. Accordingly, this study contributes to the advancement of sustainable carbon-based materials derived from renewable natural resources for emerging electrochemical sensor technologies.

2 Experimental method

2.1 Materials

Andaliman, kemuning leaves, guava leaves, and senduduk bulu were obtained from an agricultural area in North Sumatra, Indonesia. Graphite flake powder (99% carbon), ethanol, distilled water, potassium permanganate ($KMnO_4$), sulfuric acid (H_2SO_4), sodium nitrate ($NaNO_3$), hydrochloric acid (HCl) 37%, and hydrogen peroxide (H_2O_2) 30% were obtained from Sigma-Aldrich.

2.2 Preparation of extract

Powder of andaliman leaves, kemuning leaves, guava leaves, and senduduk bulu was added to ethanol 70% and stirred using a magnetic stirrer at room temperature for 1 h. The solution was then filtered to eliminate the sediment left from the extract solution.

2.3 Synthesis of graphene oxide

The synthesis of GO was performed using a modified Hummers method, as reported by Gea et al. (2022) (Gea et al. 2022). The process consisted of the following steps: A mixture of 69 mL H_2SO_4 and 3 g graphite powder was stirred in an ice bath. Subsequently, 1.5 g $NaNO_3$ was gradually added and stirred for 30 min while maintaining ice bath conditions. Then, 9 g $KMnO_4$ was slowly introduced, with the reaction temperature carefully controlled below 20 °C, and stirring continued for 2 h. The reaction vessel was then removed from the ice bath, and stirring was continued at 35 °C for 20 h. Following this, 150 mL of deionized water was slowly added, resulting in a significant exothermic reaction. This mixture was stirred for 30 min in an oil bath, ensuring the temperature did not exceed 98 °C. After removing the oil bath, the reaction was cooled in a water bath for 10 min. Subsequently, 420 mL of distilled water was added, followed by 3 mL of H_2O_2 (30%), and the mixture was stirred for 30 min, during which the reaction turned yellowish-brown. The resulting product was filtered and washed with 5% HCl to remove metal ions, followed by thorough rinsing with distilled water to eliminate residual acid. Finally, the sample was dried at 60 °C for 12 h to obtain solid GO.

2.4 Synthesis of reduced graphene oxide

The synthesis of rGO was carried out using various green reducing agents. The process involved the following steps: First, 0.1 g of GO was added to 80 ml of the green reducing agent extract. The mixture of GO and the green extract was continuously stirred for 24 h while maintaining the temperature at 80 °C. After stirring, the resulting sample was centrifuged and washed several times with distilled water (DW), followed by vacuum drying at 60 °C overnight. The dried sample was ground into powder form and stored for further analysis. The samples were designated as rGO-A (rGO from andaliman extract), rGO-K (rGO from kemuning leaf extract), rGO-G (rGO from guava leaf extract), and rGO-SB (rGO from senduduk bulu leaf extract).

2.5 Material characterization

The physicochemical properties of the synthesized rGO were thoroughly characterized using a series of analytical techniques. The surface morphology and elemental composition of the rGO samples were examined using a scanning electron microscope (SEM, JEOL JSM-IT700HR, South Korea) at ×25,000 magnification. A total of four rGO samples, each reduced using natural reducing agents derived from andaliman, kemuning leaves, guava leaves, and senduduk bulu, were analyzed. Crystallinity changes in the samples were assessed by powder X-ray diffraction (XRD) using a Philips X'Pert Pro diffractometer (Netherlands) with Cu Kα radiation ($\lambda = 1.541$ Å). The diffraction patterns of the four rGO samples were compared with that of unreduced GO to identify peak shifts and changes in interlayer spacing, which indicate successful reduction. Functional group analysis was conducted using Fourier transform infrared (FTIR) spectroscopy (Agilent Cary 630 FTIR spectrometer, USA) within the range of 4000–400 cm^{-1} to confirm the removal of oxygen-containing groups following reduction. The vibrational modes of the compounds were examined using Raman spectroscopy (Thermo Scientific DXR Raman microscope, USA, 532 nm laser excitation source). The UV–visible absorption spectra of the samples were recorded using a UV–Vis spectrophotometer (Janway 7135, UK) in the range of 200–800 nm to investigate changes in electronic conjugation after reduction. Additionally, porosity and surface characteristics, including surface area, pore volume, and pore diameter, were measured using a surface area analyzer (Quantachrome QUADRASORB SI, USA) based on the Brunauer–Emmett–Teller (BET) method. This analysis confirmed the mesoporous nature of the synthesized rGO. All characterizations were performed on four different rGO samples, while the original GO sample was used as a reference for comparison.

2.6 Electrochemical measurements

The electrochemical behavior of all rGO was investigated by cyclic voltammetry (CV) using a potentiostat (Ossila Potentiostat, UK) in 0.005 M $K_3Fe(CN)_6$/0.1 M KCl solution. Scan rate study of the modified electrodes was performed by CV in 0.005 M $K_3Fe(CN)_6$/0.1 M KCl solution by varying the scan rate from 10 mV/s to 40 mV/s.

3 Results and discussion

3.1 Structural analysis

The X-ray diffraction (XRD) patterns of GO and various rGO samples are shown in Fig. 1. The characteristic peak of GO is observed at around 2θ = 11.04°, corresponding to the (001) plane, indicating an increased interlayer spacing (d-spacing) of 8.01 Å. The expansion and broadening of the GO peak confirm the successful oxidation process, attributed to the addition of oxygen-containing functional groups between the graphite layers (Qin et al. 2019; A. Muhammad Afdhal Saputra,, et al. 2025). A small diffraction peak at 45.41° (100) is associated with the presence of minor graphite phases and incomplete exfoliation of graphite (Verma et al. Nov. 2022).

After reduction, the 2θ peak of GO shifts to 2θ = 21.79°, 24.34°, 26.00°, and 23.71° for rGO-A, rGO-K, rGO-SB, and rGO-G, corresponding to the (002) plane with interlayer spacing of 4.29 Å, 3.65 Å, 3.42 Å, and 3.75 Å, respectively. This shift indicates the removal of oxygen-containing functional groups from the rGO layers (Wu et al. 2018; Das et al. 2021). Additionally, a 2θ peak around 42° is still present in the rGO samples, though with lower intensity compared to GO. This peak is a characteristic feature that indicates turbostratic disorder in carbon materials (Chadha et al. Dec. 2021). The lower intensity suggests the formation of few-layer graphene nanosheets, which correlates with a reduction in efficiency of less than 100% (Fatimah et al. 2022; Das et al. 2021).

3.2 Functional group analysis

The nature and presence of various functional groups in GO and different rGO samples were investigated using FTIR spectroscopy. Figure 2 shows the FTIR spectra of GO and the various rGO samples. The FTIR spectrum of GO exhibits -OH stretching and C = O stretching at 3439 cm^{-1} and 1633 cm^{-1}, respectively, indicating the presence of some water molecules in the GO (Aliyev et al. 2019). Peaks at 2923 cm^{-1}, 1740 cm^{-1}, and 1252 cm^{-1} are attributed to the asymmetric stretching of aliphatic C–H, C–O stretching, and epoxy C–O stretching vibrations, respectively. Additionally, the peak at 1026 cm^{-1} corresponds to C–O (alkoxy) stretching.

Following the reduction process, the C–O (alkoxy) stretching vibrations decreased, with peaks observed at 1026 cm^{-1} for different rGO samples. These results support the reduction of GO to rGO. Furthermore, the peaks associated with -OH stretching were lower at 3439 cm^{-1} for different rGO samples, due to the removal of hydroxyl groups (Fatimah et al. 2022; Arabpour et al. 2021). The peaks at 1578 cm^{-1} are attributed to C = C (aromatic) (Longo et al. 2020). Compared to GO, all corresponding peaks in rGO displayed lower transmittance, indicating the partial elimination of oxygen-containing functional

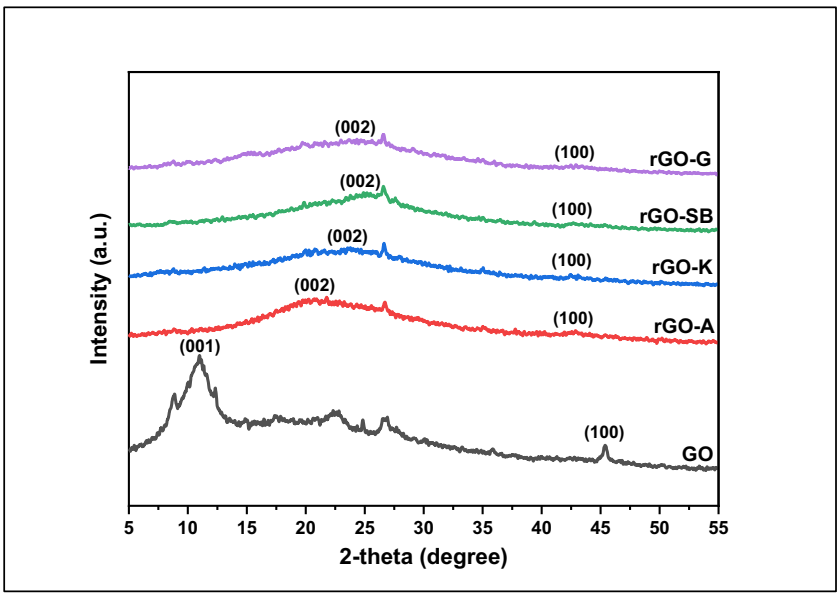


Fig. 1 XRD pattern of GO and different rGO samples

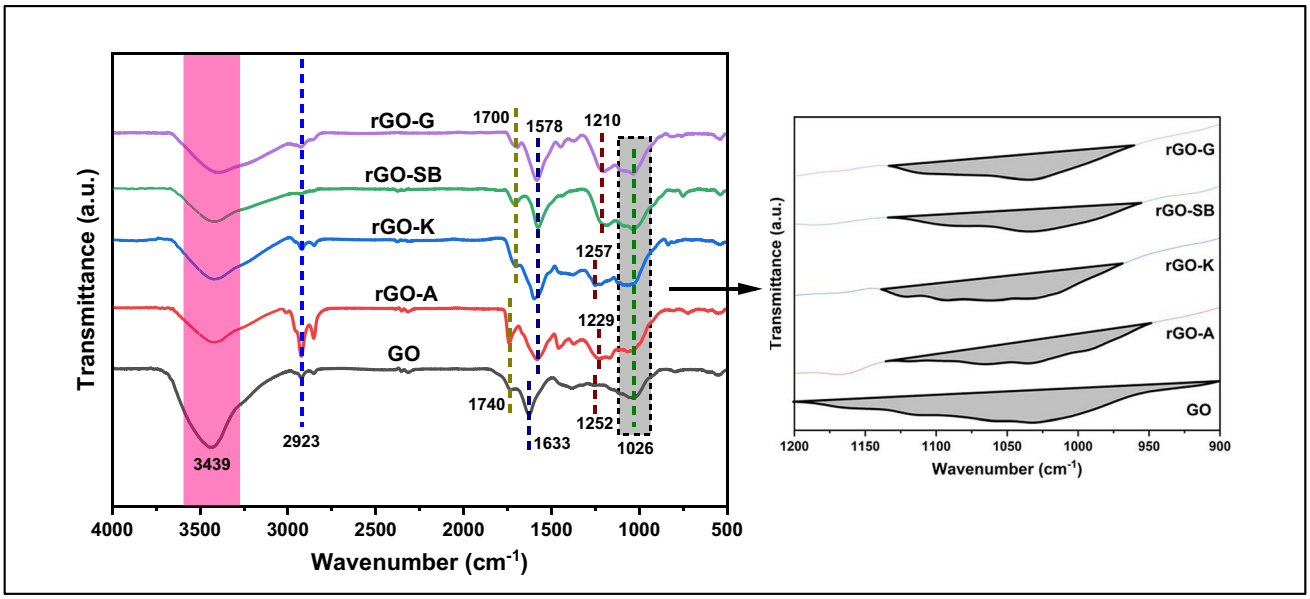


Fig. 2 FTIR spectra of GO and different rGO samples

groups (Aragaw 2020). Based on the primary and secondary metabolites present in various green reducing agents, the removal of oxygenated functional groups occurs through a reduction mechanism. For instance, the reduction process can be facilitated by polyphenolic compounds, as illustrated in Fig. 3.

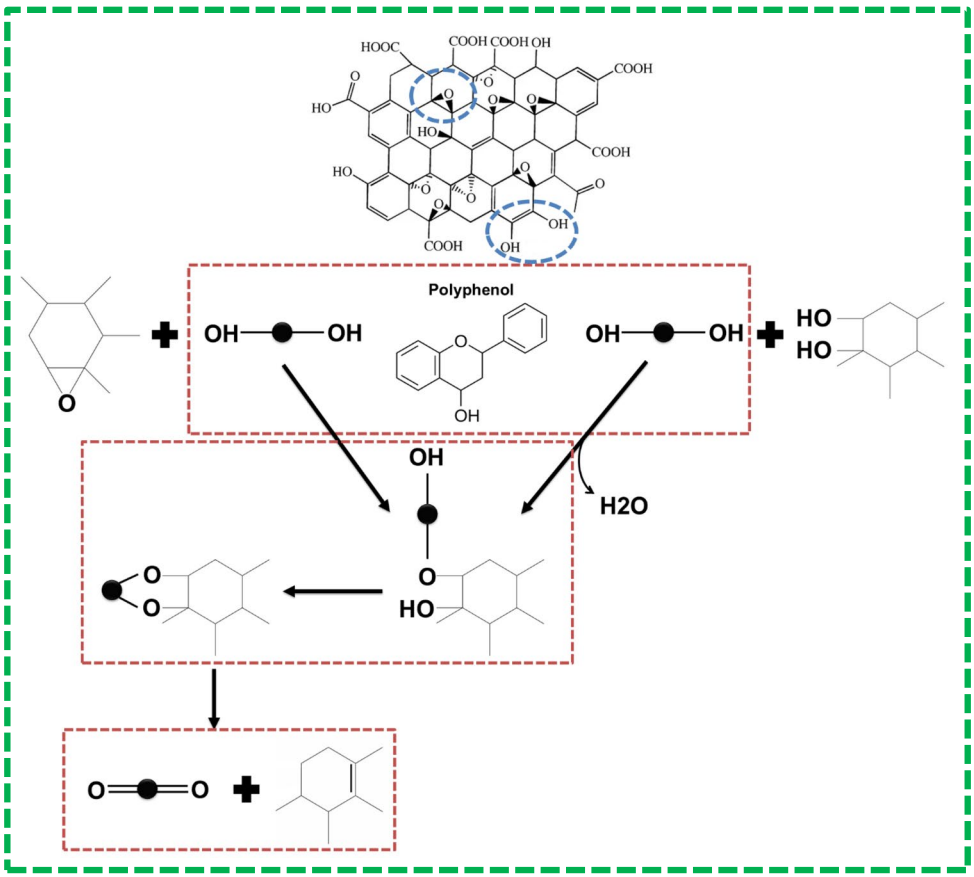


Fig. 3 Reduction mechanism of GO by polyphenolic compounds. Adapted from Fatimah et al. (2022) (Fatimah et al. 2022)

Referring to the study by Bhattacharya et al. (2017), the reduction efficiency can be measured based on the peak area around 1026 cm^{-1}, which corresponds to the C–O stretching vibration (Bhattacharya et al. 2017), using the following Eq. (Chandra Mohan Kurmarayuni, Krishna Kumari, Srikanth, and Kurapati 2024):

$$Reduction\ efficiency\ \% = \left(\frac{A_{GO} - A_{rGO}}{A_{GO}}\right) \times 100 \quad (1)$$

where A_{GO} is the area under the peak for GO, and A_{rGO} is the area under the peak for rGO. The reduction efficiency calculated for the various green reducing agents is listed in Table 1. It can be observed that the reduction efficiency is 52.27%, 42.28%, 52.63%, and 47.45% for rGO-A, rGO-K, rGO-SB, and rGO-G, respectively. This indicates that the oxygen content decreases as a result of the reduction reaction by secondary metabolites from natural extracts, which act as green reducing agents on the hydroxyl groups in GO (Khan et al. 2014). These reduction efficiency values are quite similar to those obtained using *Aloe vera* and *Annona muricata* leaf extracts as bio-reductants (Fatimah et al. 2022; Bhattacharya et al. 2017).

3.3 Raman spectroscopy

Figure 4 shows the Raman spectra of GO and BC/GO samples, demonstrating the peak shift and intensity ratio of GO to the BC/GO composite. The GO Raman spectrum indicated that the D and G peaks were located at 1342 and 1595 cm^{-1}, respectively. The D and G peaks correspond to C–H sp^3 and C–H sp^2 carbon bond structures, respectively. Additionally, the G peak signified the presence of an extended C–C bond—typical of sp^2 carbon. The two main characteristic D band and G band in rGO were shifted slightly left due to the presence of oxygen-containing functional groups, preventing the graphene layer from stacking. Due to the increase in defects and sp^2 carbon rebuilding, the relative intensity ratio I_D/I_G increases after the reduction of GO. The I_D/I_G ratios were 0.92, 0.98, 0.99, 1.03, and 1.01 for GO, rGO-A, rGO-K, rGO-SB, and rGO-G, respectively (King et al. 2016).

Table 1 Reduction efficiency of rGO synthesis using different green reducing agents

Sample	Green reducing agents	Reduction efficiency (%)	Ref
GO	-	-	This work
rGO-A	Andaliman extracts	50.27	This work
rGO-K	Kemuning leaf extracts	42.28	This work
rGO-SB	Senduduk bulu leaf extracts	52.63	This work
rGO-G	Guava leaf extracts	47.45	This work
rGO-AV	*Aloe vera*	72.51	Bhattacharya et al. 2017)
rGO-AME	Annona muricata leaf extracts	86.85	Fatimah et al. 2022)

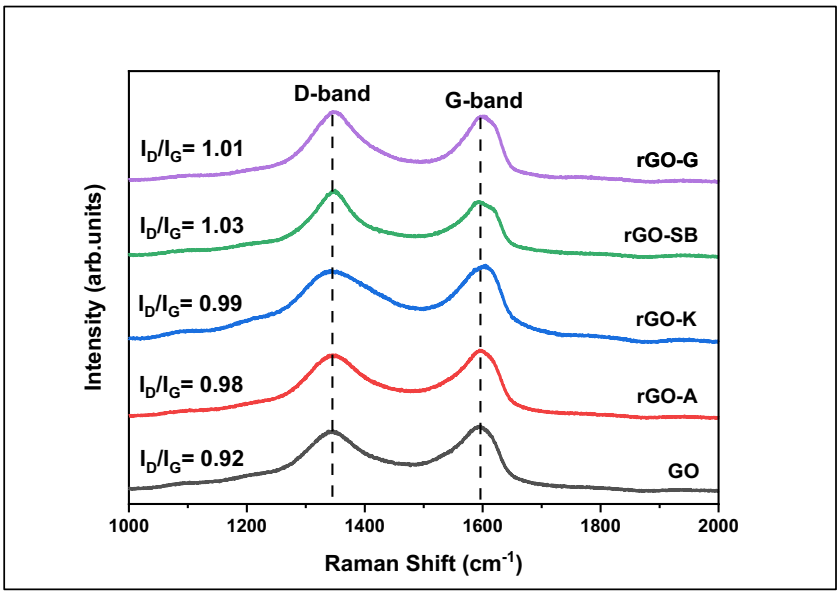


Fig. 4 Raman spectra of GO and different rGO samples

3.4 UV–visible absorption

The UV–visible absorbance spectra of GO and various rGO samples are shown in Fig. 5(a). The pure GO exhibits a significant absorption peak at 223 nm, corresponding to the $\pi \rightarrow \pi^*$ transitions of C = C bonds (Verma et al. Nov. 2022; Sujiono et al. Dec. 2023). After the green reduction process, the absorption peaks of GO shift to 267, 231, 267, and 277 nm for rGO-A, rGO-K, rGO-SB, and rGO-G, respectively. This shift is attributed to the deoxygenation process that converts GO into rGO. The changes in absorption peaks across the different rGO samples are due to $n \rightarrow \pi^*$ electron transitions, leading to a redshift in the UV–Vis absorption spectrum. This redshift indicates an increased electron concentration and the restoration of electronic conjugation within the graphene structure following the green reduction process (Verma et al. Nov. 2022; Khan et al. 2024).

The UV–Vis characterization results were subsequently analyzed using the Tauc plot method to determine the bandgap energy values for GO and the various rGO samples. According to the Wood and Tauc method, the bandgap energy can be calculated in terms of absorbance and photon energy using the following Eq. (Farooq, et al. 2024):

$$(\alpha \mathrm{hv})^2 = A(hv - Eg) \tag{2}$$

where the absorption coefficient is given by $\alpha = 2.302 \log(T/d)$ (with d being the sample thickness and T the transmission), hv is the photon energy, A is a constant, and E_g is the bandgap energy (Sujiono et al. Dec. 2023; Sujiono, et al. 2020). Using this approach, the optical bandgap of GO was found to be 3.98 eV, while the optical bandgaps for rGO-A, rGO-K, rGO-SB, and rGO-G were 3.18 eV, 3.22 eV, 3.14 eV, and 3.28 eV, respectively, as shown in Fig. 5(b). Since rGO has a lower energy gap, it results in a broader absorption range in the visible part of the electromagnetic spectrum, enhancing rGO's light-harvesting capabilities (Aragaw 2020; Tene, et al. 2023).

3.5 Morphological analysis

The surface morphology of GO and rGO was analyzed using scanning electron microscopy (SEM) to investigate the structural transformations during the reduction process. The SEM image of GO (Fig. 6a) reveals a characteristic layered and stacked structure, which is commonly observed in GO due to the presence of abundant oxygen-containing functional groups such as hydroxyl, epoxy, and carboxyl groups. These groups enhance the hydrophilicity and interlayer interactions of GO, leading to a compact, thick morphology with significant restacking of the layers (Chawla et al. 2024).

In contrast, the SEM images of rGO (Fig. 6b–e), reduced using various green reducing agents, exhibit pronounced morphological changes. These include the appearance of exfoliated, wrinkled, and crumpled sheets with fewer stacked

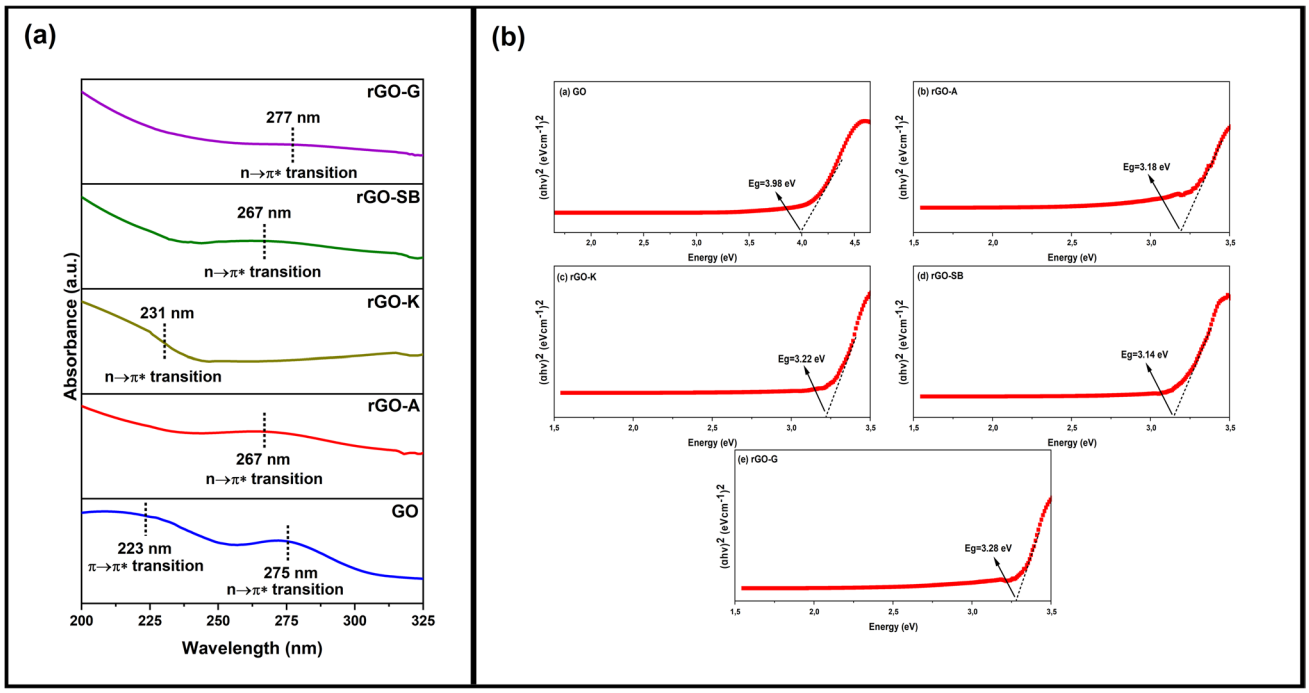


Fig. 5 (**a**) UV–visible spectra of GO and different rGO samples, and (**b**) bandgap energy of GO and different rGO samples

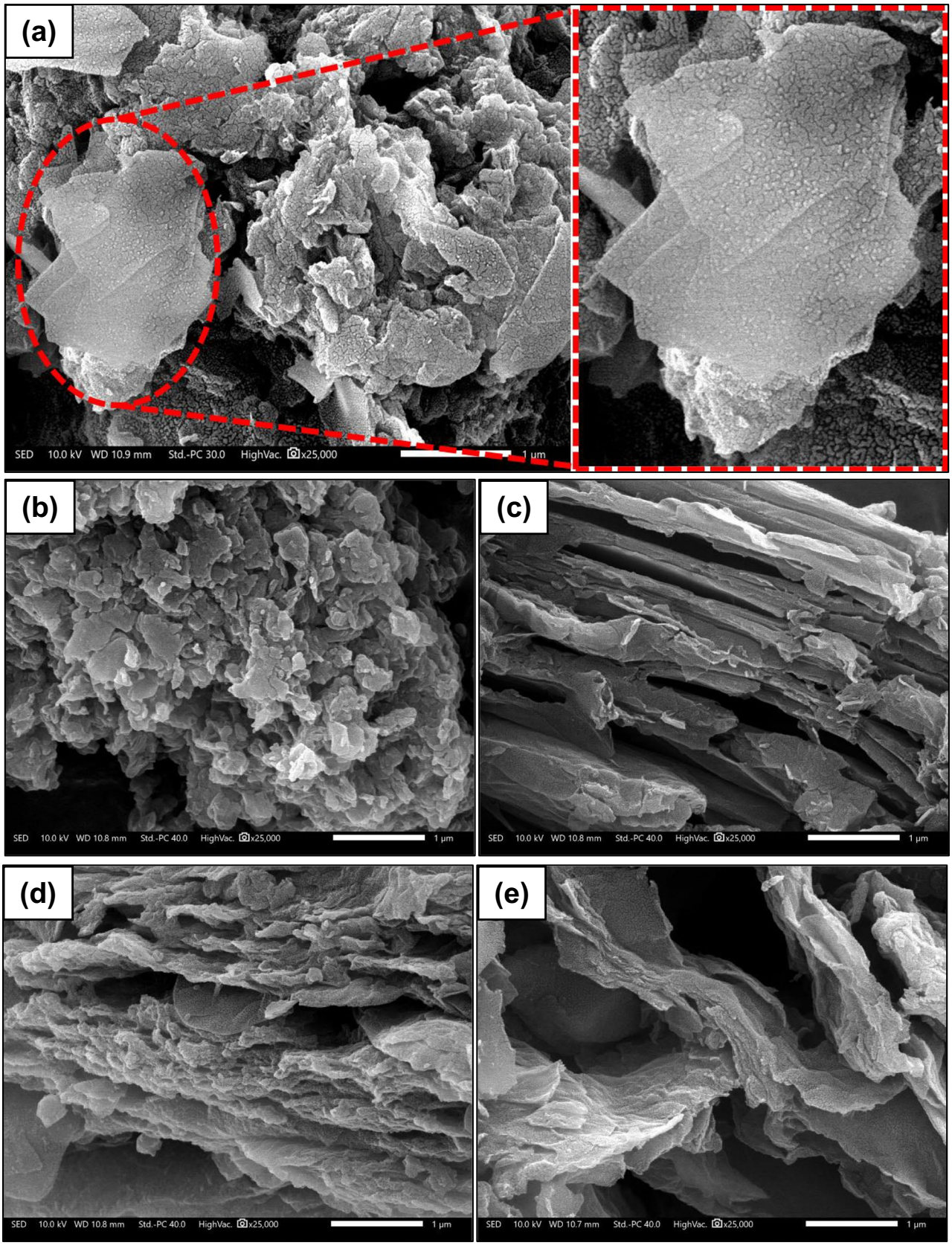


Fig. 6 SEM images of **(a)** GO, **(b)** rGO-A, **(c)** rGO-K, **(d)** rGO-G, and **(e)** rGO-SB

layers and increased surface roughness. Such structural transformations indicate the partial or complete removal of oxygen-containing groups (Kholib and Liu 2023; Gnanasekaran and Snekhalatha Nov. 2024), as also corroborated by FTIR analysis. The wrinkled and aggregated morphology of rGO reflects the reformation of the conjugated sp^2-carbon framework and the collapse of the GO sheets into thinner, more flexible graphene-like layers due to the loss of hydrophilic groups (Khan et al. 2024; Hidayah, et al. 2017; Chamoli et al. 2020). The reduction mechanism (as illustrated in Fig. 3) typically involves electron transfer from the green reducing agents to GO, leading to the cleavage of C–O bonds and restoration of C = C bonds within the carbon framework (Aunkor et al. 2016). Unlike chemical reductants like hydrazine, green reducing agents offer a milder and environmentally friendly alternative, often incorporating antioxidant molecules that can simultaneously reduce and stabilize the resulting graphene sheets (Nawaz et al. 2023; Feng et al. 2013).

The observed morphological features of exfoliation, transparency, and structural flexibility are crucial indicators of successful reduction. These characteristics contribute to enhanced electrical conductivity, mechanical strength, and surface area, which are highly desirable in various advanced applications such as flexible electronics and electrochemical sensor technologies. Therefore, the observed differences between GO and rGO underscore not only the effectiveness of the reduction process but also the capability of green reducing agents in tailoring the microstructure of rGO to meet specific functional requirements.

3.6 N_2 adsorption–desorption analysis

N_2 physisorption analysis was conducted to evaluate the specific surface area using the BET method (S_{BET}), pore diameter (D_p), and pore volume (V_p) of GO and rGO. The GO sample exhibited high adsorption capacity at low relative pressure (P/P_0), with nearly overlapping isotherms (Fig. 7a), demonstrating a specific surface area value of 997.617 m2/g. This result aligns with theoretical expectations, as the specific surface area of GO typically ranges from 500 to 1200 m2/g (Mengting et al. Dec. 2019; Dervin et al. Jun. 2017). The sample displayed an average pore diameter of 3.224 nm (as shown in Fig. 7c) and a pore volume of 1.609 cc/g. According to the IUPAC classification, this isotherm corresponds to type IV with an H3 hysteresis loop (Natarajan et al. 2018). These characteristics indicate the successful synthesis of GO with desirable porosity properties, which are crucial for various applications requiring high-surface-area materials.

In contrast, N_2 physisorption isotherms of all rGO samples demonstrated lower adsorption capacity and minimal variation compared to GO. These isotherms were classified as type II isotherms and possess hysteretic loops of type H3 (Fig. 7b). The type II isotherm suggests the absence of micropores or small mesopores in the rGO samples (Shen et al. 2018). The BET surface areas for all rGO isotherms were relatively small: rGO A (59.067 m2/g), rGO-K (46.675 m2/g), rGO-G (22.344 m2/g), and rGO-SB (33.487 m2/g). These results clearly demonstrate that the specific surface area of rGO is smaller than that of GO due to the removal of oxygen-containing functional groups during reduction, which diminishes the overall surface area and alters the material structure (Zhang et al. 2020).

The average pore diameters were measured at 2.706 nm for rGO-A, 3.490 nm for rGO-K, 4.202 nm for rGO-G, and 3.540 nm for rGO-SB. The pore volumes were determined to be 7.992 cc/g for rGO-A, 8.146 cc/g for rGO-K, 4.695 cc/g for rGO-G, and 5.928 cc/g for rGO-SB, indicating the presence of larger pores relative to GO (Table 2). The pore diameter distribution was nearly indistinguishable among all rGO samples (Fig. 7d). All synthesized rGO samples exhibited mesoporous characteristics with pore diameters ranging from 2 to 50 nm (Natarajan et al. 2018), with an average pore diameter of approximately ± 3 nm. The mesoporous structure of rGO plays a crucial role in enhancing the electrochemical performance of the material, particularly in electron transfer processes (Zeng et al. 2017). The presence of medium-sized pores (2–50 nm) in rGO significantly increases the specific surface area, which in turn increases the number of electrochemically active sites available for redox reactions (Kong et al. Aug. 2013; Mao et al. 2016). This supports a higher efficiency of electron transfer between the electrode surface and the electroactive species in the solution.

Through experimental data analysis, it was found that when P/P_0 was in the range of 0.05–0.35, the linear fitting (as reported in Fig. 8) yielded highly satisfactory results. The correlation coefficient ($R2$) values demonstrated exceptional fitting accuracy, with GO achieving $R2 = 0.999192$, while the rGO samples exhibited values of $R2 = 0.999592$ for rGO-A, $R2 = 0.998642$ for rGO-K, $R2 = 0.999782$ for rGO-G, and $R2 = 0.999709$ for rGO-SB. These remarkably high correlation coefficients indicate excellent agreement between the experimental data and the BET model, thereby ensuring accurate determination of the specific surface area (Cao et al. 2021). The BET constant (C), which is related to the adsorption energy, was calculated from the slope (s) and intercept (i) of the linear plots. Higher BET constants typically indicate stronger adsorbate–adsorbent interactions (Kostoglou, et al. 2024), as observed in the cases of rGO-G and rGO-A. This finding suggests that these two rGO variants exhibit enhanced surface interaction capabilities, potentially due to their unique surface chemistry and structural characteristics resulting from the reduction process.

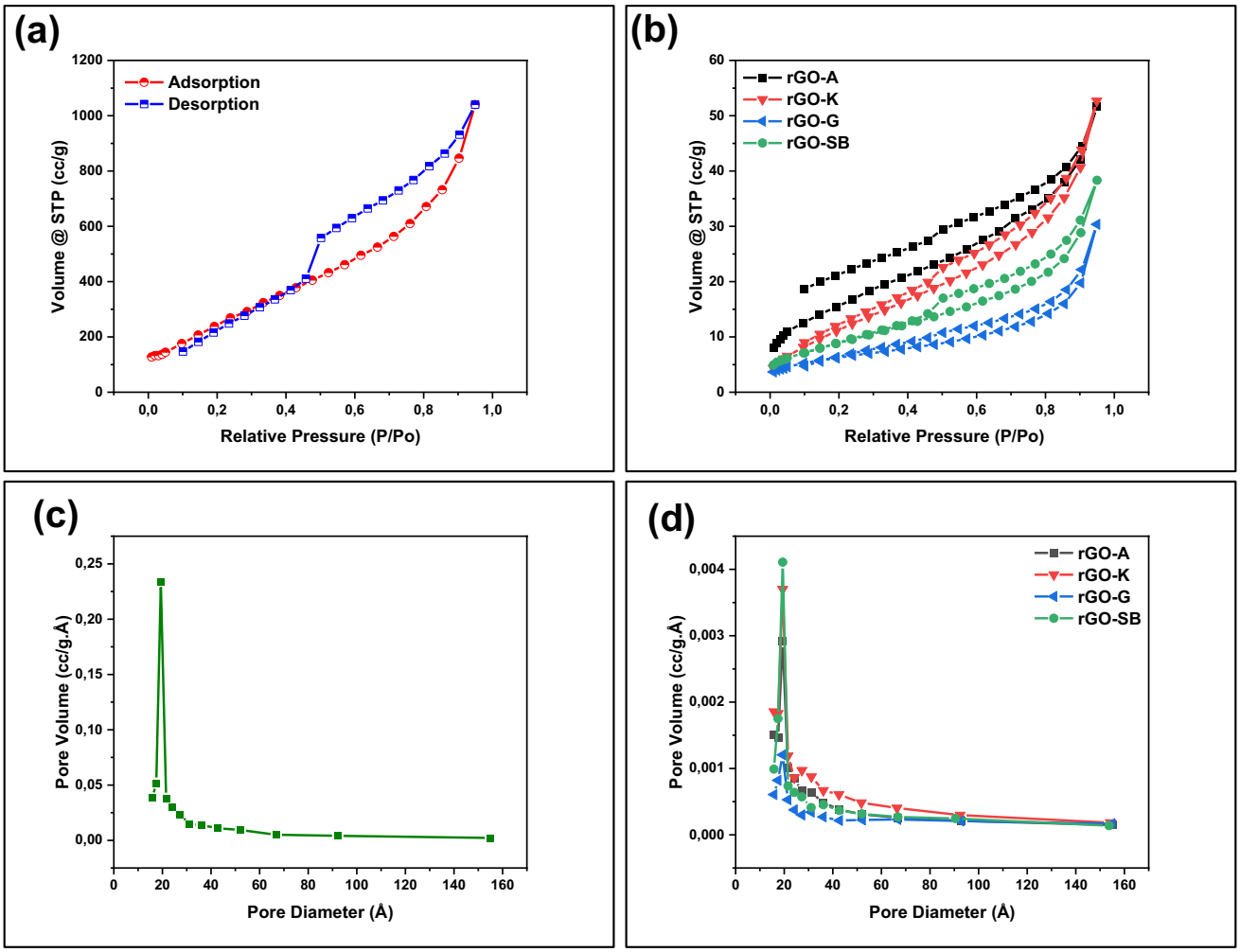


Fig. 7 The N_2 adsorption–desorption isotherm plots of **(a)** GO and **(b)** different rGO samples. The pore size distribution results calculated from the Barrett–Joyner–Halenda (BJH) desorption pore volume data for **(c)** GO and **(d)** different rGO samples

Table 2 Textural properties of GO and different rGO samples. The textural properties were calculated based on N_2 physisorption results

Sample	Green reducing agents	S_{BET} (m^2/g)[a]	D_p (nm)[b]	V_p (cc/g)[c]
GO	-	997.617	3.224	1.609
rGO-A	Andaliman extracts	59.067	2.706	7.992
rGO-K	Kemuning leaf extracts	46.675	3.490	8.146
rGO-SB	Senduduk bulu leaf extracts	22.344	4.202	4.695
rGO-G	Guava leaf extracts	33.487	3.540	5.928

[a]Specific surface area calculated by the BET method

[b]Average pore diameter following the Gurvich rule

[c]Total pore volume calculated at $P/P_0 = 0.95$

3.7 Electrochemical study

The electrochemical behavior of all rGO samples was evaluated using cyclic voltammetry (CV) in a 0.005 M $K_3[Fe(CN)_6]$ solution containing 0.1 M KCl, with measurements conducted at a scan rate of 40 mV/s within a potential range of − 0.4 V to 0.8 V. The electrocatalytic reaction on the electrode surface can be outlined as follows:

$$[Fe(CN)_6]^{-4} \rightarrow [Fe(CN)_6]^{-3} + e \text{ (oxidation)} \quad (3)$$

$$[Fe(CN)_6]^{-3} + e \rightarrow \left[Fe(CN)_6\right]^{-4} \text{(reduction)} \quad (4)$$

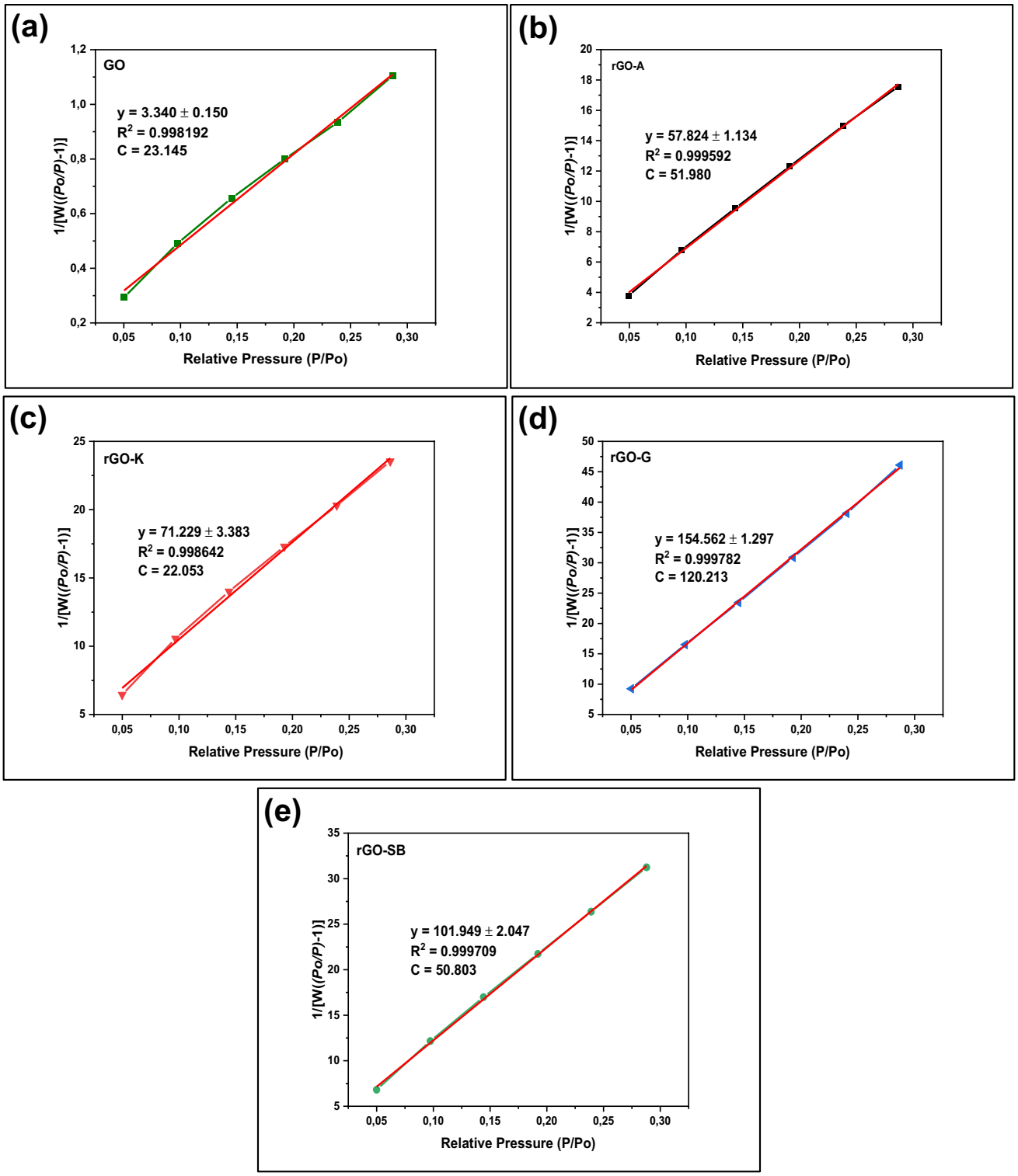


Fig. 8 Multi-point BET of **(a)** GO, **(b)** rGO-A, **(c)** rGO-K, **(d)** rGO-G, and **(e)** rGO-SB

Equations (Jovanovic, et al. 2024) and (T. N 2024) represent the anodic/cathodic peaks obtained in the CV curves. As shown in Fig. 9a, the CV profiles of all rGO samples at a scan rate of 40 mV/s exhibit a quasi-reversible wave shape (Xinsheng and Guogang 1987; Guziejewski et al. 2022). This indicates a reversible redox process, where the oxidation and reduction peak potentials are closely spaced, and the midpoint between these peaks

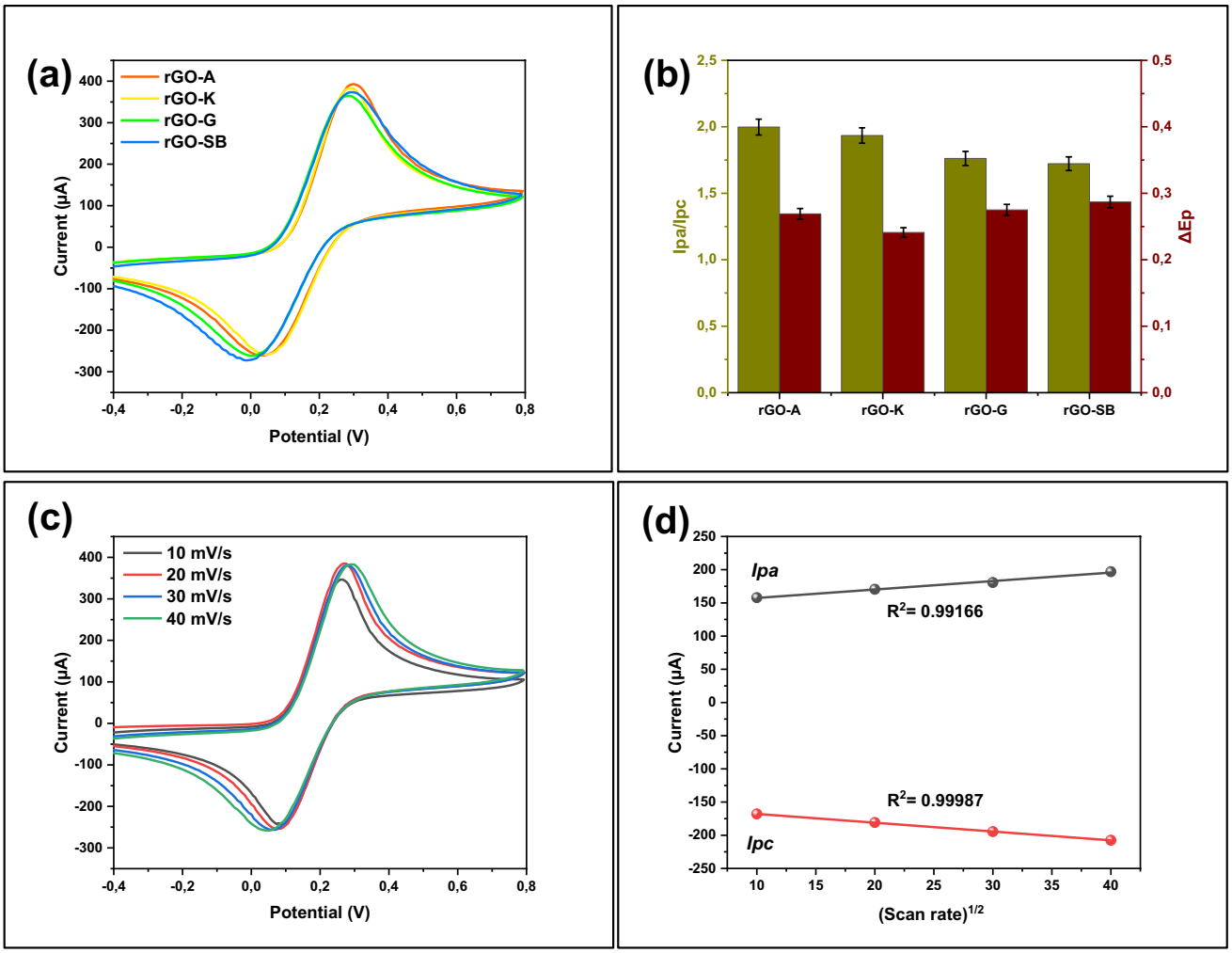


Fig. 9 (**a**) The CV curves, (**b**) ΔE_p and (I_{pa}/I_{pc}) of different rGO samples (the error bars represent the standard deviation calculated based on the average results collected from three trials); (**c**) CV of rGO-SB with scan rate variation; (**d**) the current density vs. (scan rate)$^{1/2}$ plot

corresponds to the redox potential of the electroactive species (Kissinger and Heineman 1983). These results are consistent with the study conducted by Huan et al. (2012), who successfully synthesized rGO via a chemical reduction route. Their work also demonstrated a reversible redox process with distinct redox peaks (Huan et al. Aug. 2012), indicating similarities in the electrochemical characteristics between the material synthesized in this study and those reported previously.

The reversible CV shape can be explained by the following mechanism: Initially, at lower applied potentials, the energy is insufficient to initiate electron transfer, resulting in negligible or no detectable current (Oldham 2013). As the applied potential increases in the positive direction, the current gradually rises, indicating the onset of electron transfer at the electrode surface. The current subsequently reaches a maximum value as the reaction rate approaches its peak due to the availability of redox-active species at the electrode interface (Kosala. Wijeratne 2018). This behavior can be further understood through the intrinsic structure of rGO. Graphene, a two-dimensional sp2-hybridized carbon nanosheet, possesses abundant localized π electrons. When used as an electrode modifier for sensing applications, graphene can interact with aromatic analyte species via π–π conjugation, leading to their adsorption on the graphene surface. According to this adsorption mechanism, the extent of restoration of the sp2-hybridized graphitic network in rGO—governed by the energy applied during the reduction process—directly influences the strength of π–π interactions. Therefore, the superior electron transfer behavior and redox performance observed in rGO samples can be attributed not only to their high conductivity and large surface area, but also to their enhanced π-electron system that facilitates both redox activity (Li et al. 2015).

In addition, the values of ΔEp and I_{pa}/I_{pc} were also evaluated in this study (Fig. 9b), where theoretically, the

Table 3 The electrochemically active surface area values of all different rGO samples

Sample	Green reducing agents	Electrochemically active surface area (cm^2)
rGO-A	Andaliman extracts	0.0264
rGO-K	Kemuning leaf extracts	0.0402
rGO-G	Guava leaf extracts	0.0416
rGO-SB	Senduduk bulu leaf extracts	0.0384

optimal ΔEp is approximately 0.24, and the optimum I_{pa}/I_{pc} is approximately 1. The I_{pa}/I_{pc} values for all rGO samples were found to range from 1.722 to 1.997, while the ΔEp values were within the range of 0.24–0.29. These findings indicate that the redox reaction in this system is not entirely reversible and likely falls into the category of quasi-reversible (Pajkossy and Vesztergom 2019), which is consistent with the CV profile shown in Fig. 9a. This behavior is likely attributable to several determining factors, such as significant electron/mass transfer capabilities, a large number of surface-active reaction sites due to the presence of S vacancies, extremely low resistance, and excellent conductivity, as confirmed by BET analysis (large surface area) (Satra et al. 2023). With these advantages, the rGO in this study demonstrates significant potential for further development as an electrode material in electrochemical sensor systems.

The optimal sample, rGO-SB, was selected for determining the electrochemically active surface area (ECSA), and CV measurements were performed at varying scan rates ranging from 10 to 40 mV/s under similar reaction conditions (Fig. 9c). The peak current was observed to increase progressively with higher scan rates. The asymptotic line observed in the plot of peak current density versus the square root of the scan rate adhered well to the Randles–Sevcik Eq. 51 (Eq. (Yip and Tong 2023)), which was used to calculate the ECSA values of the samples (Table 3). These results clearly highlight that the highest ECSA and the surface architecture of rGO-K had a significant impact on its exceptional electrocatalytic performance.

$$I_p = 2.69 \times 10^5 \, n^{3/2} A D^{1/2} C g^{1/2} \tag{5}$$

where I_p represents the peak current density, n is the number of transferred electrons, A denotes the ECSA of the working electrode, D is the diffusion coefficient of the electrolyte, C is the concentration of the $[Fe(CN)_6]^{3-/4-}$ ions, and g represents the operating scan rate. Figure 9d shows the anodic and cathodic peak currents (I_{pa} and I_{pc}) plotted against the square root of the scan rate. Linear behavior is observed, with $R2$ values of 0.99166 for I_{pa} and 0.99987 for I_{pc}. This linearity suggests excellent charge carrier mobility based on a diffusion-controlled process (Ching et al. 2021). Thus, this work advances the sustainable production of graphene-based materials for next-generation electrochemical sensors.

4 Conclusions

This study presents a novel and eco-conscious approach to synthesizing high-quality reduced graphene oxide (rGO) using natural reducing agents extracted from andaliman, kemuning leaves, guava leaves, and senduduk bulu—plants native to Indonesia and largely unexplored in nanomaterial research. The successful reduction of graphene oxide was confirmed by a suite of advanced characterization techniques. XRD and FTIR analyses evidenced effective structural transformation and a substantial removal of oxygen-containing groups, with reduction efficiency reaching as high as 52.63%. UV–Vis spectroscopy further confirmed enhanced π–π* transitions, while SEM revealed the formation of characteristic wrinkled, exfoliated rGO sheets. BET analysis validated the mesoporous nature of the materials, with pore diameters ideal for electrochemical applications. Most notably, electrochemical studies demonstrated superior electron transfer kinetics, supported by excellent linearity in peak current responses ($R2 > 0.99$), suggesting efficient charge transport properties. The integration of green chemistry principles with nanomaterial synthesis highlights the originality and environmental relevance of this work. By utilizing naturally sourced plant extracts as sustainable reducing agents, this method offers a scalable and nontoxic alternative to conventional reduction techniques—paving the way for greener production of graphene-based materials in electrochemical sensor technologies.

Acknowledgements The authors are thankful to the Indonesian Ministry of Education, Culture, Research and Technology for providing financial support through the PMDSU research scheme with Grant No. 90/UN5.4.10.S/PPM/KP-DRTPM/2024.

Authors contribution **A. Muhammad Afdhal Saputra:** Writing–original draft, Visualization, Software, Resources, Methodology, Investigation, Formal analysis, Data curation, Conceptualization. **Marpongahtun:** Writing–review & editing, Supervision, Validation. **Andriayani:** Writing–review & editing, Supervision, Validation. **Ronn Goei:** Writing–review & editing. **Alfred Tok:** Writing–review & editing. **Stergios Goutianos:** Writing–review & editing, Validation, Supervision. **Saharman Gea:** Writing–review & editing, Validation, Supervision, Resources, Methodology, Investigation, Funding acquisition, Conceptualization.

Data availability The data that has been used is confidential.

Declarations

Competing interest The authors declare that they have no known competing financial interests or personal relationships that could have appeared to influence the work reported in this paper.

Open Access This article is licensed under a Creative Commons Attribution 4.0 International License, which permits use, sharing, adaptation, distribution and reproduction in any medium or format, as long as you give appropriate credit to the original author(s) and the source, provide a link to the Creative Commons licence, and indicate if changes were made. The images or other third party material in this article are included in the article's Creative Commons licence, unless indicated otherwise in a credit line to the material. If material is not included in the article's Creative Commons licence and your intended use is not permitted by statutory regulation or exceeds the permitted use, you will need to obtain permission directly from the copyright holder. To view a copy of this licence, visit http://creativecommons.org/licenses/by/4.0/.

References

Alam SN, Sharma N, Kumar L (2017) Synthesis of Graphene Oxide (GO) by Modified Hummers Method and Its Thermal Reduction to Obtain Reduced Graphene Oxide (rGO)*. Graphene 06(01):1–18. https://doi.org/10.4236/graphene.2017.61001

Aliyev E, Filiz V, Khan MM, Lee YJ, Abetz C, Abetz V (2019) Structural characterization of graphene oxide: Surface functional groups and fractionated oxidative debris. Nanomaterials 9(8): https://doi.org/10.3390/nano9081180

Amir Faiz MS, Che Azurahanim CA, Raba'ah SA, Ruzniza MZ (2020) Low cost and green approach in the reduction of graphene oxide (GO) using palm oil leaves extract for potential in industrial applications. Results Phys. 16: 102954. https://doi.org/10.1016/J.RINP.2020.102954

Anju M, Renuka NK (2019) Graphene–dye hybrid optical sensors. Nano-Structures and Nano-Objects 17:194–217. https://doi.org/10.1016/j.nanoso.2019.01.003

Arabpour A, Dan S, Hashemipour H (2021) Preparation and optimization of novel graphene oxide and adsorption isotherm study of methylene blue. Arab J Chem 14(3):103003. https://doi.org/10.1016/J.ARABJC.2021.103003

Aragaw BA (2020) Reduced graphene oxide-intercalated graphene oxide nano-hybrid for enhanced photoelectrochemical water reduction. J Nanostructure Chem 10(1):9–18. https://doi.org/10.1007/s40097-019-00324-x

Asih R et al. (2019) Comparative study on magnetism of reduced graphene oxide (Rgo) prepared from coconut shells and the commercial product. In: Materials Science Forum, Trans Tech Publications Ltd. pp. 290–295. https://doi.org/10.4028/www.scientific.net/MSF.966.290

Aunkor MTH, Mahbubul IM, Saidur R, Metselaar HSC (2016) The green reduction of graphene oxide. Royal Soc Chem. https://doi.org/10.1039/c6ra03189g

Baqiya MA et al (2020) Structural study on graphene-based particles prepared from old coconut shell by acid–assisted mechanical exfoliation. Adv Powder Technol 31(5):2072–2078. https://doi.org/10.1016/J.APT.2020.02.039

Bhattacharya G, Sas S, Wadhwa S, Mathur A, McLaughlin J, Roy SS (2017) Aloe vera assisted facile green synthesis of reduced graphene oxide for electrochemical and dye removal applications. RSC Adv 7(43):26680–26688. https://doi.org/10.1039/c7ra02828h

Brodie BC (1960) Sur le poids atomique du graphite. Annales De Chimie Et De Physique 59:466–472

Cao N, Wang G, Liang Y (2021) Study on the Microscopic Mechanism of Spontaneous Combustion and Oxidation Kinetics of Water-Leached Coal. J Chem 2021. https://doi.org/10.1155/2021/5564290.

Chadha N, Sharma R, Saini P (2021) A new insight into the structural modulation of graphene oxide upon chemical reduction probed by Raman spectroscopy and X-ray diffraction. Carbon Letters 31(6):1125–1131. https://doi.org/10.1007/s42823-021-00234-5

Chamoli P, Banerjee S, Raina KK, Kar KK (2020) Characteristics of Graphene/Reduced Graphene Oxide," in *Handbook of Nanocomposite Supercapacitor Materials I: Characteristics*, K. K. Kar, Ed., Cham: Springer International Publishing. pp. 155–177. https://doi.org/10.1007/978-3-030-43009-2_5.

Chandra Mohan Kurmarayuni A, Krishna Kumari P, Srikanth B, Kurapati S (2024) Chapter 15 graphene: synthetic and reduction approaches futuristic trends in chemical. 3(3)

Chawla K, Sharma PS, Lal N, Rathore BS, Lal C (2024) Synthesis of Graphene Oxide by Modified New Hummer Method. Macromol Symp. 413(5):2400179. https://doi.org/10.1002/masy.202400179

Chen C, Chen YC, Hong YT, Lee TW, Huang JF (2018) Facile fabrication of ascorbic acid reduced graphene oxide-modified electrodes toward electroanalytical determination of sulfamethoxazole in aqueous environments. Chem Eng J 352:188–197. https://doi.org/10.1016/J.CEJ.2018.06.110

Ching CB, Abdullah J, Yusof NA (2021) Reduced Graphene Oxide/Gold Nanoparticles Modified Screen-Printed Electrode for the Determination of Palmitic Acid. J Sens 2021. https://doi.org/10.1155/2021/6684770.

Chong SW, Lai CW, Abdul Hamid SB (2015) Green preparation of reduced graphene oxide using a natural reducing agent. Ceram Int 41(8):9505–9513. https://doi.org/10.1016/j.ceramint.2015.04.008

Das P, Deoghare AB, Maity SR (2021) A Novel Approach to Synthesize Reduced Graphene Oxide (RGO) at Low Thermal Conditions. Arab J Sci Eng 46(6):5467–5475. https://doi.org/10.1007/s13369-020-04956-y

Dervin S, Lang Y, Perova T, Hinder SH, Pillai SC (2017) Graphene oxide reinforced high surface area silica aerogels. J Non Cryst Solids 465:31–38. https://doi.org/10.1016/J.JNONCRYSOL.2017.03.030

Faniyi IO et al. (2019) The comparative analyses of reduced graphene oxide (RGO) prepared via green, mild and chemical approaches. SN Appl Sci. 1(10): https://doi.org/10.1007/s42452-019-1188-7

Farooq N et al. (2024) Graphene Oxide and Based Materials: Synthesis, Properties, and Applications – A Comprehensive Review. MatSci Express. 1(4):185–231. https://doi.org/10.69626/mse.2024.0185

Fatimah I, Fadillah G, Ayu Rednasari R, Wahyuningsih S (2022) Green reduction of graphene oxide using Annona muricata leaves extract for adsorption of methylene blue. Inorg Chem Commun. 146:110144. https://doi.org/10.1016/J.INOCHE.2022.110144

Feng Y, Feng N, Du G (2013) A green reduction of graphene oxide via starch-based materials. RSC Adv 3(44):21466–21474. https://doi.org/10.1039/c3ra43025a

Gea S et al (2022) Facile synthesis of ZnO–Ag nanocomposite supported by graphene oxide with stabilised band-gap and wider visible-light region for photocatalyst application. J Market Res 19:2730–2741. https://doi.org/10.1016/j.jmrt.2022.05.184

Gnanasekaran B, Snekhalatha U (2024) Exploring Reduction Techniques for Graphene Oxide: A Comparative Study of Thermal and Chemical Methods. ChemistrySelect 9(43):e202403827. https://doi.org/10.1002/slct.202403827

Guziejewski D, Stojanov L, Gulaboski R, Mirceski V (2022) Reversible and Quasireversible Electron Transfer under Conditions of Differential Square-Wave Voltammetry. J Phys Chem C 126(12):5584–5591. https://doi.org/10.1021/acs.jpcc.2c01188

Hidayah NMS et al. (2017) Comparison on graphite, graphene oxide and reduced graphene oxide: Synthesis and characterization," in *AIP Conference Proceedings*, American Institute of Physics Inc. https://doi.org/10.1063/1.5005764.

Huan TN, Van Khai T, Kang Y, Shim KB, Chung H (2012) Enhancement of quaternary nitrogen doping of graphene oxide via chemical reduction prior to thermal annealing and an investigation of its electrochemical properties. J Mater Chem 22(29):14756–14762. https://doi.org/10.1039/c2jm31158e

Hummers WS, Offeman RE (1958) Preparation of Graphitic Oxide. J Am Chem Soc 80(6):1339. https://doi.org/10.1021/ja01539a017

Jovanovic S et al. (2024) Carbon-Based Nanomaterials in Electromagnetic Interference Shielding: Graphene Oxide, Reduced Graphene Oxide, Electrochemically Exfoliated Graphene, and Biomass-Derivated Graphene. In: 2024 International Conference on Manipulation, Automation and Robotics at Small Scales (MARSS). pp. 1–5. https://doi.org/10.1109/MARSS61851.2024.10612734

Khan M et al (2014) Pulicaria glutinosa plant extract: A green and eco-friendly reducing agent for the preparation of highly reduced graphene oxide. RSC Adv 4(46):24119–24125. https://doi.org/10.1039/c4ra01296h

Khan MU, Shaida MA (2023) Reduction mechanism of graphene oxide including various parameters affecting the C/O ratio. Mater Today Commun 36:106577. https://doi.org/10.1016/J.MTCOMM.2023.106577

Khan A, Sapakal SN, Kadam A (2024) Comparative analysis of graphene oxide (GO) reduction methods: impact on crystallographic, morphological, and optical properties,. Graphene 2D Mat 9(1–2):101–109. https://doi.org/10.1007/s41127-024-00072-y.

Kholib NS, Liu WW (2023) Graphene Synthesis by Electrochemical Reduction of Graphene Oxide and Its Characterizations

King AAK et al (2016) A new Raman metric for the characterisation of graphene oxide and its derivatives. Sci Rep 6:1–6. https://doi.org/10.1038/srep19491

Kissinger PT, Heineman WR (1983) Cyclic voltammetry. J Chem Educ 60(9):702. https://doi.org/10.1021/ed060p702

Kosala. Wijeratne (2018) *Conducting Polymer Electrodes for Thermogalvanic Cells*. Linkopings Universitet

Kong Q-Q, Chen C-M, Zhang Q, Zhang X-H, Wang M-Z, Cai R (2013) Small Particles of Chemically-Reduced Graphene with Improved Electrochemical Capacity. The Journal of Physical Chemistry C 117(30):15496–15504. https://doi.org/10.1021/jp403497u

Kostoglou N et al. (2024) The Roles of Impurities and Surface Area on Thermal Stability and Oxidation Resistance of BN Nanoplatelets. Nanomaterials 14(7): https://doi.org/10.3390/nano14070601

Kumar P et al (2021) Utilization of green reductant Thuja Orientalis for reduction of GO to RGO. Ceram Int 47(10):14862–14878. https://doi.org/10.1016/J.CERAMINT.2020.08.063

Kumar R et al (2023) Graphene-based materials for biotechnological and biomedical applications: Drug delivery, bioimaging and biosensing. Mater Today Chem 33:101750. https://doi.org/10.1016/J.MTCHEM.2023.101750

Kumari N, Bhandari M (2024) Surface Functionalization Reactions of Graphene-Based Nanostructure and Their Practical Application. In: Chemistry of Graphene, E. W. Wambu, Ed., Rijeka: IntechOpen. p. Ch. 3. https://doi.org/10.5772/intechopen.114855.

Jin X, Li N, Weng X, Li C, Chen Z (2018) Green reduction of graphene oxide using eucalyptus leaf extract and its application to remove dye. Chemosphere 208:417–424. https://doi.org/10.1016/J.CHEMOSPHERE.2018.05.199

Li S-J, Xing Y, Deng D-H, Shi M-M, Guan P-P (2015) A comparative study of different types of reduced graphene oxides as electrochemical sensing platforms for hydroquinone and catechol. J Solid State Electrochem 19(3):861–870. https://doi.org/10.1007/s10008-014-2692-8

Liu W, Speranza G (2022) Chemical Reduction of GO: Comparing Hydroiodic Acid and Sodium Borohydride Chemical Approaches by X-ray Photoelectron Spectroscopy. C-J Carbon Res 8:2. https://doi.org/10.3390/c8020020

Liu Z et al (2022) Graphene-based materials prepared by supercritical fluid technology and its application in energy storage. J Supercrit Fluids 188:105672. https://doi.org/10.1016/J.SUPFLU.2022.105672

Liu X, Shi L, Jiang W, Zhang J, Huang L (2018) Taking full advantage of KMnO4 in simplified Hummers method: A green and one pot process for the fabrication of alpha MnO2 nanorods on graphene oxide. Chem Eng Sci 192:414–421. https://doi.org/10.1016/J.CES.2018.07.044

Longo A, Palomba M, Carotenuto G (2020) Green solid-state chemical reduction of graphene oxide supported on a paper substrate. Coatings 10(7): https://doi.org/10.3390/coatings10070693

Mahalingam S, Omar A, Manap A, Rahim NA (2023) Synthesis and applications of carbon-polymer composites and nanocomposite functional materials. Functional Materials from Carbon, Inorganic, and Organic Sources: Methods and Advances. pp. 71–105. https://doi.org/10.1016/B978-0-323-85788-8.00020-3.

Mahmudzadeh M, Yari H, Ramezanzadeh B, Mahdavian M (2019) Highly potent radical scavenging-anti-oxidant activity of biologically reduced graphene oxide using Nettle extract as a green bio-genic amines-based reductants source instead of hazardous hydrazine hydrate. J Hazard Mater 371:609–624. https://doi.org/10.1016/J.JHAZMAT.2019.03.046

Makaudi R, Paumo HK, Dalhatou S, Kamdem BP, Katata-Seru L, Bahadur I (2023) Development of graphene oxide-supported nanocatalysts for reduction of nitroarenes in wastewater. Adsorption through Advanced Nanoscale Materials: Applications in Environmental Remediation. 623–645. https://doi.org/10.1016/B978-0-443-18456-7.00026-2

Mao X, Guo F, Yan EH, Rutledge GC, Hatton TA (2016) Remarkably High Heterogeneous Electron Transfer Activity of Carbon-Nanotube-Supported Reduced Graphene Oxide. Chem Mater 28(20):7422–7432. https://doi.org/10.1021/acs.chemmater.6b03024

Mengting Z et al (2019) Applicability of BaTiO3/graphene oxide (GO) composite for enhanced photodegradation of methylene blue (MB) in synthetic wastewater under UV–vis irradiation. Environ Pollut 255:113182. https://doi.org/10.1016/J.ENVPOL.2019.113182

Muhammad Afdhal Saputra A et al. (2025) Facile synthesis and electrochemical performance of bacterial cellulose/reduced graphene oxide/NiCo-layered double hydroxide composite film for self-standing supercapacitor electrode. Mater Sci Energy Technol 8:66–81. https://doi.org/10.1016/j.mset.2024.08.001

Natarajan S, Rao Ede S, Bajaj HC, Kundu S (2018) Environmental benign synthesis of reduced graphene oxide (rGO) from spent lithium-ion batteries (LIBs) graphite and its application in supercapacitor. Colloids Surf A Physicochem Eng Asp 543:98–108 https://doi.org/10.1016/j.colsurfa.2018.01.054

Nawaz MH, Iqbal N, Rehman R, Lim JW , Shahid MK (2023) Green synthesis and characterization of reduced graphene oxide. *Voprosy Khimii i Khimicheskoi Tekhnologii.* (4): 69–76. https://doi.org/10.32434/0321-4095-2023-149-4-69-76

Oldham KB (2013) Ultimate cyclic voltammetry: An analytical examination of the reversible case. J Solid State Electrochem 17(11):2749–2756. https://doi.org/10.1007/s10008-013-2176-2

Othman NH, Alias NH, Shahruddin MZ, Marpani F, Aba NFD (2022) Synthesis methods of graphene. Graphene, Nanotubes Quant Dots-Based Nanotechnol: Fundamentals Appl. 19–42. https://doi.org/10.1016/B978-0-323-85457-3.00037-2

Pajkossy T, Vesztergom S (2019) Analysis of voltammograms of quasi-reversible redox systems: Transformation to potential program invariant form. Electrochim Acta 297:1121–1129. https://doi.org/10.1016/J.ELECTACTA.2018.12.023

Panicker NJ, Sahu PP (2021) Green reduction of graphene oxide using phytochemicals extracted from Pomelo Grandis and Tamarindus indica and its supercapacitor applications. J Mater Sci: Mater Electron 32(11):15265–15278. https://doi.org/10.1007/s10854-021-06077-0

Patra S, Roy E, Tiwari A, Madhuri R, Sharma PK (2017) 2-Dimensional graphene as a route for emergence of additional dimension nanomaterials. Biosens Bioelectron 89:8–27. https://doi.org/10.1016/j.bios.2016.02.067

Qin J et al (2019) Room temperature production of graphene oxide with thermally labile oxygen functional groups for improved lithium ion battery fabrication and performance. J Mater Chem A Mater 7(16):9646–9655. https://doi.org/10.1039/c9ta02244a

Ramanathan S et al (2021) Grape Seed Extract Assisted Synthesis of Dual-Functional Anatase TiO2Decorated Reduced Graphene Oxide Composite for Supercapacitor Electrode Material and Visible Light Photocatalytic Degradation of Bromophenol Blue Dye. ACS Omega 6(23):14734–14747. https://doi.org/10.1021/acsomega.0c02325

Satra J, Mondal P, Bhadu GR, Adhikary B (2023) In situ fabrication and design of a novel electrochemical sensor based on the Ag3.84Sn3S8@rGO nanocomposite for competitive ultra-detection of metronidazole in human urine. Mater Adv 4(10):2340–2353. https://doi.org/10.1039/d3ma00076a

Shayeghi Sabzevar P, Bagheri – Mohagheghi MM, Shirpay A (2022) The effect of rGO and chemical reduction under hydrazine on the structural, electrical and optical properties of nanostructured SnO2:F/rGO thin films. Physica B Condens Matt. 646:414310 https://doi.org/10.1016/J.PHYSB.2022.414310

Shen L et al (2018) Analysis of oxidation degree of graphite oxide and chemical structure of corresponding reduced graphite oxide by selecting different-sized original graphite. RSC Adv 8(31):17209–17217. https://doi.org/10.1039/c8ra01486h

Singh PK, Singh PK, Sharma K (2023) An Electrochemical Route for the Synthesis of Low Oxygen Containing Reduced Graphene Oxide through 2B Grade Graphite. NANO 18(08):2350039. https://doi.org/10.1142/S179329202350039X

Staudenmaier L (1898) Verfahren zur Darstellung der Graphitsäure. Ber Dtsch Chem Ges 31:1488–1499. https://doi.org/10.1002/cber.18980310237

Sujiono EH et al. (2020) Graphene oxide based coconut shell waste: synthesis by modified Hummers method and characterization. Heliyon 6(8): https://doi.org/10.1016/j.heliyon.2020.e04568.

Sujiono EH et al (2023) Coconut shell waste-derived graphene oxide composite with neodymium oxide (Nd2O3) for advanced applications. Results in Materials 20:100480. https://doi.org/10.1016/J.RINMA.2023.100480

Tene T et al. (2023) Temperature-Dependent Optical Properties of Oxidized Graphenes. Nanomaterials 13(15): https://doi.org/10.3390/nano13152263

T.N. (2024) Investigation on Structural, Optical, and Thermal Properties of Graphene Oxide (GO) Nanoparticles. Int J Sci Res Eng Manag. 08(4):1–5. https://doi.org/10.55041/IJSREM30191

Verma S, Das T, Pandey VK, Verma B (2022) Facile and scalable synthesis of reduced-graphene oxide using different green reducing agents and its characterizations. Diam Relat Mater 129:109361. https://doi.org/10.1016/J.DIAMOND.2022.109361

Wu Y et al (2018) Reduction of graphene oxide alters its cyto-compatibility towards primary and immortalized macrophages. Nanoscale 10(30):14637–14650. https://doi.org/10.1039/c8nr02798f

Xinsheng C, Guogang P (1987) Cyclic square wave voltammetry: Theory and experimental. Anal Lett 20(10):1511–1519. https://doi.org/10.1080/00032718708078023

Yip TM, Tong GB (2023) Fabrication Routes of Graphene. In: Graphene: Fabrication, Properties and Applications. R. T. Subramaniam, R. Kasi, S. Bashir, and S. S. A. Kumar, Eds., Singapore: Springer Nature Singapore. pp. 53–90. https://doi.org/10.1007/978-981-99-1206-3_4.

Zeng J, Amici J, Monteverde Videla AHA, Francia C, Bodoardo S (2017) Synthesis of mesoporous carbons and reduced graphene oxide and their influence on the cycling performance of rechargeable Li-O2 batteries. J Solid State Electrochem 21 (2):503–514. https://doi.org/10.1007/s10008-016-3391-4

Zhang Z et al. (2022) Layer-by-layer growth of bilayer graphene single-crystals enabled by self-transmitting catalytic activity

Zhang S, Wang H, Liu J, Bao C (2020) Measuring the specific surface area of monolayer graphene oxide in water. Mater Lett 261:127098. https://doi.org/10.1016/J.MATLET.2019.127098

Publisher's Note Springer Nature remains neutral with regard to jurisdictional claims in published maps and institutional affiliations.